

Design and Control of Foam Hands for Dexterous Manipulation

Dominik Bauer^{*§}, Cornelia Bauer^{*¶}, Jonathan P. King^{*||},
Daniele Moro^{†***}, Kai-Hung Chang^{*††},
Stelian Coros^{*‡‡} and Nancy Pollard^{*§§}

**Robotics Institute, Carnegie Mellon University,
5000 Forbes Avenue, Pittsburgh, Pennsylvania 15213, USA*

*†Department of Computer Science,
Boise State University, 1910 University Dr.,
Boise, Idaho 83725, USA*

*‡Department of Computer Science,
ETH Zürich, Rämistrasse 101, 8092 Zürich, Switzerland*
§dominikb@andrew.cmu.edu
¶cornelib@andrew.cmu.edu
||jking2@andrew.cmu.edu
**daniellemoro@u.boisestate.edu
††kaihungc@andrew.cmu.edu
‡‡scoros@inf.ethz.ch
§§nsp@cs.cmu.edu

Received 1 April 2019
Accepted 11 November 2019
Published 6 January 2020

There has been great progress in soft robot design, manufacture, and control in recent years, and soft robots are a tool of choice for safe and robust handling of objects in conditions of uncertainty. Still, dexterous in-hand manipulation using soft robots remains a challenge. This paper introduces foam robot hands actuated by tendons sewn through a fabric glove. The flexibility of tendon actuation allows for high competence in utilizing deformation for robust in-hand manipulation. We discuss manufacturing, control, and design optimization for foam robots and demonstrate robust grasping and in-hand manipulation on a variety of different physical hand prototypes.

Keywords: Grasping and manipulation; novel mechanism design; physical interaction; soft robots; tendon-driven mechanism design; robot hands.

1. Introduction

In industrial applications, robotic systems have long been successfully applied for tasks such as loading of machines or spot welding. Reasons for this are that such tasks are highly repeatable and are usually executed within separate workspaces for

§Corresponding author.

humans and machines to avoid injuries. In contrast, future robotic systems will need to operate safely, robustly and adaptively in complex unstructured environments.

An emerging class of robots designed to address this problem are *soft robots* which are made from intrinsically soft materials. Apart from being safe, the softness and compliance achieved by these robots can be exploited to reduce the complexity of interactions with the environment. For example, the compliance of soft robots allows them to adapt to geometric variations without the need of complex low-level control. Such an exploitation of compliance can be observed in many biological organisms and is therefore a promising characteristic. Soft robots have shown great ability to conform to object surfaces, produce solid grasps, and handle fragile objects gently. However, achieving human level dexterity, including dexterous in-hand manipulation, remains a challenge.

In this paper, we introduce fully soft foam robots actuated by tendons routed through a fabric glove. Because these hands are constructed only of foam, they are lightweight and compliant. Tendons can be routed anywhere along the surface of the hand, allowing for complex families of deformations and facilitating dexterous in-hand manipulation. We demonstrate the capability of foam hands by showing power and precision grasps and in-hand dexterous manipulations on several different robot hand geometries (Fig. 1, bottom). Contributions of this paper include:

- Fabrication methodology for *foam robots*, tendon actuated soft robots, using simple molding and casting techniques and driven by servo actuated tendons;



Fig. 1. (Top) Manufacturing pipeline. (Middle) Positives from life casting, CAD designs, and algorithmic processes; a 3D printed mold. (Bottom) Hand prototypes designed and developed using this process.

- Fine-tuning and validation of a soft robot simulation framework;
- Evaluation and comparison of different control strategies for solving the inverse kinematics problem of foam robots;
- Optimization and automatic design of nontrivial tendon routings to achieve desired tasks;
- User study results demonstrating human ability to route tendons to achieve desired tasks and comparison to results from the optimization algorithm;
- Experiments and demonstrations that serve to illustrate the capabilities of these robots, such as complex manipulations, sub-millimeter repeatability, and continuing functionality over 1-year later;
- Discussion of design challenges and methodology insights that shed light on the capabilities, drawbacks, and potential of this class of robot.

This paper builds on two conference publications by the authors^{1,2} and contributes substantial new material, including an algorithm for tendon optimization (Sec. 6, Figs. 9–11), a user study to evaluate the ability of human subjects to achieve high quality tendon routings (Sec. 7, Figs. 12 and 13), additional examples, and expanded discussion throughout.

2. Related Works

Soft robotics has shown great potential for producing versatile robots for a variety of tasks³ that are inherently safe⁴ due to their compliant nature, making them ideal systems for physical human interaction.^{5–7} Over the years, there have been many interesting studies in soft robotics that explored variations in geometry,⁸ fabrication techniques,⁹ and actuation.^{10–12} Textiles, inflatables, and foams have been investigated as materials to make robots more suitable for human robot interaction scenarios.^{5,7,13} A variety of soft materials have been investigated and used in medical applications for rehabilitation,¹⁴ wearables,^{15,16} exoskeletons,¹⁷ toys,^{18,19} robots that locomote and grasp,^{20–22} flexible sensors^{23,24} and artificial skin.^{25,26}

Fluidic elastomer actuators (FEA) and electroactive polymers comprise the most commonly used actuation mechanisms in soft robotics.^{27–34} Controlled stiffness can be achieved from low-melting point alloys, shape memory materials, and granular jamming.³⁵ Controlled adhesion may be dry adhesion,³⁶ suction cups^a or electro-adhesion.³⁷ A number of fluidic elastomer actuators have successfully been used in anthropomorphic hands and grippers.^{8,21,29,38–41} Dexterous soft robot hands have been constructed.^{8,42} However, dexterous manipulation utilizing completely soft hands remains a novel field and a grand challenge.

Most tendon-driven soft robots combine rigid links with elastic hinges.^{43–45} Completely soft tendon-driven systems have been developed as well,^{20,46,47} although this technology is not commonly applied to soft robot hands. The research most closely related to ours is the work by Bern *et al.*¹⁹ who developed tendon-driven plush

^aFesto Co. Ltd. Octopus Gripper.

robots using textiles. However, these robots are intended as toys for children, and are not suitable for dexterous manipulation. We move to use a cast foam interior, rather than stuffing, to improve deformation behavior and structure in more complex 3D geometries. Furthermore, we investigate new fabrication techniques that make use of well-developed practices from the artistic prop and textile industries.

In terms of soft robot hand control, previous works have particularly studied the problem of inverse kinematics (IK).^{48–50} Model-based controllers rely on the establishment of a kinematic model from which the actuation can be directly inferred for the desired configuration.^{39,51–54} Model-free approaches utilize data to fit models to observed behavior.^{49,55} We compare a set of alternative approaches to determine the most accurate approach to use for modeling the foam robots introduced in this paper.

For optimization of soft robots, Deimel and colleagues⁵⁶ propose a co-design method that simultaneously optimizes morphology and control of a pneumatically actuated soft hand. Reiffel *et al.*⁵⁷ search for morphology, material and control parameters. Other research concerned with optimizing material parameters has been introduced by Hiller *et al.*,⁵⁸ who obtain locomotion of their designs by finding heterogeneous material distributions with the help of evolutionary algorithms. Inouye and colleagues⁵⁹ optimize anthropomorphic tendon-driven robotic hands containing rigid links, focusing on improving the grasp quality of the designs and show that robotic hands can even exceed human grasping. Our paper explores a similar approach in the context of optimizing tendon routings on a fully soft robot hand.

3. Fabrication

We present in this section, a set of fabrication techniques and mechanisms used to create a soft multi-fingered hand. To achieve the goal of “true” softness, the robot is constructed of only soft foams, knitted textile skins, fibrous tendons, and flexible PTFE tubes for cable routing. All rigid mechanical components are housed away from the hand. To make the process easily accessible to nonexperts, the fabrication methodology was chosen to be low-cost (< \$100), and relies on easy to follow casting techniques that can be readily found in step by step internet video tutorials. The mechanical devices we use consist of off-the-shelf components, 3D-printed parts, and laser cut acrylic, and so should also be accessible to the novice user.

Creating the Mold. A hand geometry and posture is chosen, evaluated in simulation, and fine-tuned prior to manufacture. We have used life casting, algorithmic techniques, and CAD software to produce these initial hand geometries (Fig. 1, middle). Using the hand geometry the user can either create a mold around a physical representation of the hand (or an actual human hand) or utilize CAD software or automatic mold generation methods^{60,61} to yield models that can be 3D-printed or machined.

Casting Foam Hands. A two-part urethane foam compound is used to cast the final foam hand. A variety of densities are available; we most preferred *FlexFoam-iT! X*,

finding it a good balance of strength and compliance. The behavior of the foam is not always intuitive: while casting humanlike hands we found that slightly thicker sections of the palm were much stiffer, and slightly thinner sections of the fingers were much softer. Therefore, the hand geometry should be carefully considered to avoid unwanted behavior. While not necessary, the use of a laboratory mixing machine guarantees very consistent results from cast to cast. We are able to go from a chosen rest pose or model to a cast foam hand in under 24 h for a cost of approximately \$50 for the mold and only a few dollars for each foam hand afterward.

Gloves and Sewing Tendons. A textile exterior, e.g., a glove, is used as a skin for the foam hand, acting as a layer conducive to sewing in tendons for actuation. For anthropomorphic hands, off the shelf gloves can be used, but for general soft robots, sewn skins from cut felt can be used. In our case, gloves were custom knit for each hand geometry using automatic processes.⁶² The custom gloves can be knit in under an hour with many choices of materials, greatly complementing our rapid prototyping approach. Whatever choice of skin is selected, it is then laminated to the foam core to prevent slip using spray-on upholstery adhesive.^b Tendons are realized in practice with PTFE coated braided fishing line, and are sewn into the glove with a typical sewing needle, and fixed at the ends with finishing knots.

Robot Chassis. The gloved hand is fixtured to a laser-cut acrylic base with hot-melt glue. The tendons are routed through PTFE tubes along the base of the hand to minimize friction where they then interface with servo driven winches. Additional mounting points are placed on the acrylic base so that the PTFE tubes can be fixtured with cable ties. The assembly is detailed in Fig. 1, top.

4. Simulation

Because they are comprised of uniform flexible material, the foam hands made using our process can be well simulated using standard finite element techniques (FEM). We utilize these simulations for interactive design, control, optimization, and learning. For the simulation, we follow the approach of Bern *et al.*¹⁸ who use a finite element model to capture the deformation behavior of soft plush toys. We transfer their representation of soft plushies consisting of a series of contractile elements (modeled as stiff unilateral springs) to our foam hands. Each foam hand is modeled as a discrete set of nodes denoted as \mathbf{x} for the statically stable deformed pose. The total deformation energy of the system is defined as

$$E = E_{\text{foam}} + E_{\text{contractile}} + E_{\text{pins}},$$

where E_{foam} is the energy due to deformations of the simulation mesh, $E_{\text{contractile}}$ is the strain energy stored by the contractile elements, and E_{pins} models the behavior of stiff springs that connect a small number of simulation nodes to world anchors in order to

^b3M Adhesive 23.

Table 1. Material properties used in FEM simulation.

ρ [kg/m ³]	E [Pa]	ν
160	3e6	0.25

eliminate rigid body modes. The elastic behavior of the foam is modeled using linear finite elements with a compressible Neo-Hookean material model.

Tendons are modeled as *contractile* elements that abstract the contraction of a tendon as changing the rest length of the underlying unilateral spring model. A contractile element is defined as a piecewise linear curve with two endpoints (x_s, x_t) and n intermediate vertices (x_1, \dots, x_n). We assume that all points of contractile elements are bound to nodes of the simulation mesh. The initial rest length l_0 of a tendon is defined by the sum of distances between the vertices as

$$l_0 = \|x_s - x_1\| + \sum_{i=1}^{n-1} \|x_i - x_{i+1}\| + \|x_n - x_t\|.$$

The contraction level α_c of each tendon describes the contracted length as

$$l_c = l_0 \cdot (1 - \alpha_c).$$

In the following, the word *routing* refers to the choice of endpoints and intermediate vertices of each tendon. The resulting deformation for a tendon routing with the contractions α_c is calculated by minimizing the total energy of the system using Newton's method. A detailed description of this step and the calculation of deformation energy can be found in the work by Bern *et al.*¹⁸ We tuned simulation parameters through observed visual feedback to match qualitative behavior of the foam hands in simulation with the behavior of physical hands. The obtained values of the material parameters are shown in Table 1 and are validated with motion capture data in Sec. 8.

5. Control, and Learning

The softness and flexibility of the foam hand is advantageous for secure grasping and robust in-hand manipulation. However, working with such a hand requires the application of new modeling and control techniques.

Telemanipulation: Learning on the Robot. In the most basic scenario, we have only the robot itself, with a given arrangement of tendons and motors, and a device with which the user wishes to control the robot. With this equipment, we must learn a mapping from user gestures or poses to motor actuations that deform the robot in the desired manner. We explore a straightforward mapping, where the user wears a *CyberGlove* and controls an anthropomorphic hand that is similar to their own. However, we wish to allow for flexibility when the geometries of the human and robot hands may differ significantly.

We take inspiration from research on puppeteering in computer graphics. For example, Seol and colleagues⁶³ present a method that allows the user to specify how they wish to move in order to create certain character motions. As an example, they might choose to swing their arm to move an elephant's trunk. In the case of Seol *et al.*,⁶³ an approach based on feature mapping is used to convert from user motion to character control parameters. In our case, we use linear regression to create a map from *CyberGlove* sensors to tendon activations for the hand.

Our approach works as follows. First, a sampling of tendon activations is used to execute various poses of the foam hand. An operator imitates those poses while wearing the calibrated *CyberGlove*, and the corresponding joint angles of the human hand pose are recorded. Both random tendon activations and tendon activations corresponding to finger-thumb oppositions and grasping postures were used to build a training set of 120 hand poses. For generalization purposes, each pose was recorded 5 times.

A regression model, which takes the 22 joint angles from the *CyberGlove* as input and predicts the corresponding tendon activation levels was trained. The model uses *Kernel Ridge Regression* with a linear kernel. The average RMS error achieved by the model between the measured and the predicted normalized tendon actuations was 0.0026, with normalized tendon actuation ranging from zero to one. A normalized actuation value of zero refers to a loose tendon and a value of one specifies the maximum actuation, which was set individually for each tendon by qualitative observation.

Even with a small training set (120 recordings), the learned model was able to reproduce a variety of poses with high accuracy based on qualitative evaluation. Figure 2 shows a comparison of poses supplied by an operator and the poses realized by the foam hand. Both poses taken from the training set and new poses are included.

We note that in order to achieve such results, the careful selection of training poses is crucial. While our first approach was to sample poses with only one finger contracted at a time, we gained the insight that especially for coupled motions such a

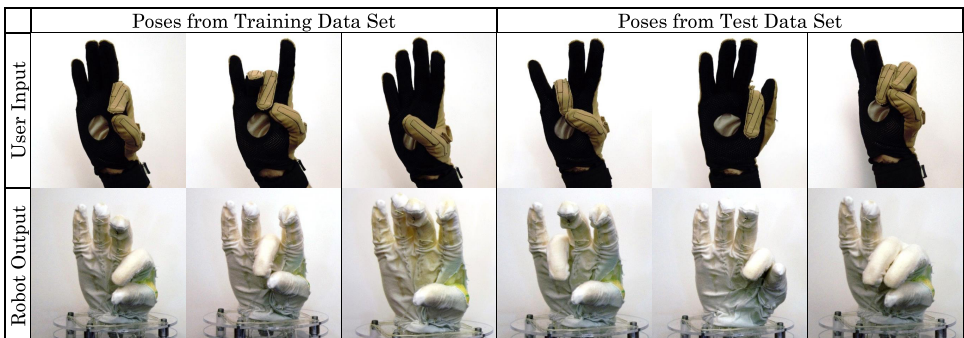


Fig. 2. (Top) Input poses from user wearing a *CyberGlove*. (Bottom) Output poses from the learned mapping. (Left) Poses taken from the training set. (Right) Poses not included in the training set.

model does not generalize well. In terms of posing this means that fingertips of opposing fingers do not touch or align for example. Adding specific poses that include coupled tendon contractions, as shown in the trained poses of Fig. 2 can significantly increase generalization. Therefore we suggest to use poses that are related to the task that needs to be executed. Using just three additional task-specific poses (shown in Fig. 2 on the left) the learned mapping was also precise enough to perform telemanipulation tasks, including grasping objects and in-hand manipulations. Since during the described sampling process we rely exclusively on the person wearing the *CyberGlove* to match the robot poses with their hand, this approach may be influenced by subjective impression of how well poses match. A strong advantage of this technique however is the possibility to easily create mappings between the human hand and different hand morphologies. Given that the human operator can create a corresponding hand pose for each robot hand pose, this technique can even be applied to nonanthropomorphic foam hands.

Learning in Simulation. Learning on the robot is straightforward and was successful. However, the amount of test data that can be collected is limited and similarity in poses is only qualitative and depends on the patience, care, and point of view of the user. If we can learn a mapping from poses to actuations in simulation, the comparison between test poses and learned poses can be much more exact, and we can explore how additional data may improve the results.

Collecting data in simulation is faster and easier than collecting data on the physical robot. Making use of the accessibility of large amount of data from the simulation, we are able to apply learning-based methods with complex models. These methods take the concatenated fingertip positions as the input and output the tendon activation that is expected to pose the hand correspondingly. Four different methods are applied and compared: (1) nearest neighbor; (2) linear ridge regression; (3) neural network using supervised learning; and (4) deep reinforcement learning.

The **Nearest neighbor** method serves as a straw-man approach. It takes the tendon activation of the pose that is nearest to the desired pose in the pose space based on Euclidean distance and simply returns that tendon activation as the result. **Linear ridge regression** is supplied in part because it was used for learning for telemanipulation as previously described. It is perhaps the second simplest sensible approach beyond Nearest neighbor. We use a linear model with an additional L2 ridge regularizer. A **neural network using supervised learning** adds additional degrees of freedom and nonlinearity. We include this model to determine whether the additional complexity can improve fit to the data. Our neural network model is constructed with four intermediate layers, each of which has 30 units and ReLU nonlinear activations. The activation of the output layer is $\tanh(x)$ to match a linear-normalized range $[-1, 1]$ of the output activation. The training process runs 300 epochs with a batch size of 20, a learning rate of 0.001 and Adam optimizer with the typical parameter values ($\alpha = 0.001$, $\beta_1 = 0.9$, $\beta_2 = 0.999$, $\epsilon = 1 \times 10^{-8}$). **Deep reinforcement learning** can be considered as an alternative approach to learning a



Fig. 3. Anthropomorphic foam hand prototype in its rest pose. (Left) physical foam hand prototype, (Middle) Scan of the prototype, (Right) Finite element mesh used in simulation.

nonlinear model. Based on the success of learning IK on both rigid robot arms and hands,⁶⁴ deep reinforcement learning is expected to transfer to soft robots. In particular, we apply the deep deterministic policy gradient⁶⁵ algorithm combined with hindsight experience replay.⁶⁶ The shaped reward function is the negative of the average distance error over all fingers. Hindsight experience replay can be considered as a way to include additional targeted results, as “failed” solutions are reinterpreted during learning as successful solutions to a different problem.

A simulation model of the physical anthropomorphic foam hand shown in Fig. 3 (Left) is obtained by using *Autodesk ReMake*⁶⁷ to generate a surface mesh from approximately 50 images of the hand taken with a smartphone. We then run *TetGen*⁶⁸ to build a 3D finite element mesh of the hand, shown in Fig. 3 (Right).

To compare the sample efficiency of all four methods, we use the same datasets for both training and testing. The training dataset collects 100,000 poses while the testing dataset contains 100 poses, all of which are pre-generated in the simulation by drawing randomly from possible tendon activations.

We plot the performance (average distance error in centimeters) with respect to the amount of data used in training. The comparison plot is shown in Fig. 4. When training with less than 100,000 samples, the training data is extracted in sequence from the large 100,000 dataset. The plot shows that linear ridge regression is outperformed by all other approaches especially for large datasets, implying that additional model complexity is useful for this test dataset. Overall, and to our surprise, the nearest neighbor method shows the best performance and the best sample efficiency. However, results from nearest neighbor approaches are typically not smooth for datasets that do not comprehensively cover the space of tendon actuations. Lastly, deep reinforcement learning outperforms supervised learning. The main difference between these two approaches lies in the meaning of the loss functions. In supervised learning, the network is trained to fit the target tendon activations from the training data, hoping that the trained model can be generalized to unseen poses. In contrast, the objective of reinforcement learning is to maximize reward and thus

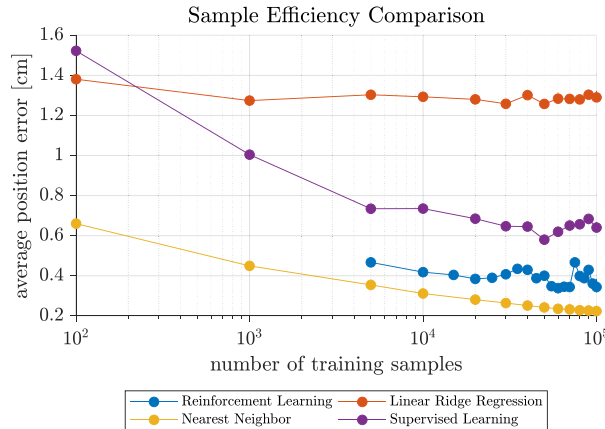


Fig. 4. Performance of four different methods to learn IK in simulation.

directly minimize the average distance error. As a result, the loss function used in reinforcement learning has better expressiveness for our ultimate learning task-matching the target pose. For example, reinforcement learning can adapt to a situation where some tendon activation levels show greater sensitivity than others for changing the final target pose and thus should be learned with greater accuracy.

Another reason is that reinforcement learning learns from sequential steps. Though the policy network performs poorly at the beginning of learning, every single step it takes can be used to improve itself thanks to the actor-critic mechanism. Furthermore, the usage of hindsight experience replay provides richer information from unsuccessful steps; unsuccessful steps in effect are added to the training set, providing additional information for learning the final mapping from pose to activation levels.

6. Tendon Optimization

The previous section showed that we can use the simulation to learn a mapping from tendon activations to hand deformations given a foam hand morphology and a tendon routing. However, defining a useful tendon routing is not an easy task.

We build a tendon optimization approach around the idea of randomly placing a number of tendons on the hand mesh, contracting them and comparing the resulting pose to the desired goal pose. As core algorithm we use a Metropolis–Hastings–Algorithm,^{69,70} which either accepts or rejects such a randomly sampled tendon routing based on its deviation from a goal pose. To deal with the large amount of local minima, we additionally introduce Simulated Annealing which adopts the concept of cooling a temperature. This allows the algorithm to accept solutions in the early stages that are worse than previous solutions and thus, escape local minima.

While the temperature T is larger than a minimum temperature T_{\min} the algorithm iteratively modifies its current state, calculates the associated costs and then either accepts or rejects the new state. We define a state using the tuple $\mathcal{S}_k = \{\mathbf{x}, \mathcal{T}, \mathcal{A}\}$ with \mathbf{x} containing the nodal positions of the contracted mesh, \mathcal{T} the set of tendons and \mathcal{A} the set of contractions.

Initialization. A tendon t is represented by a number of waypoints $\{\hat{x}_0, \dots, \hat{x}_n\}$ along which it is routed. We term such points *anchoring nodes* in the following. For each tendon the optimization is initialized by sampling n anchoring nodes from a discrete uniform distribution $\mathcal{U}(0, N)$ with N being the number of nodes in the mesh. After sampling, the corresponding tendon is placed on the mesh by connecting the anchoring nodes along the shortest path on the mesh. The initial contraction level α_0 of each tendon is a hyperparameter with values ranging from 0.0 to 1.0.

Creating New States. To create new states we sample a new tendon routing \mathcal{T}_{k+1} and new contraction levels \mathcal{A}_{k+1} simultaneously. To create new tendon routings, one anchoring node from each tendon is sampled based on a heuristic that prefers transitions to adjacent nodes over transitions to nodes that are located further away.

This is realized by creating a set of neighboring nodes \mathcal{M}_k which are in direct or close adjacency to the anchoring node that is being changed. First, the adjacency depth $d \sim \mathcal{U}(0, D)$ is sampled from a discrete uniform distribution, with the maximum depth D serving as a hyper-parameter. Then all nodes which are located within this adjacency are added to the set \mathcal{M}_k . Finally, the new anchoring node is sampled uniformly from \mathcal{M}_k .

In addition to sampling anchoring nodes, new contraction levels \mathcal{A}_{k+1} are created by sampling variations δ from a normal distribution $\delta \sim \mathcal{N}(0.0, 0.05)$ and applying them to the current contraction levels as follows:

$$\mathcal{A}_{k+1} = \mathcal{A}_k + \delta. \quad (1)$$

Evaluating Candidate Solutions. Our main goal is to obtain tendon routings that can achieve certain grasps, thus the cost η_t of a state is primarily evaluated in terms of whether one or several goal poses are achieved. Each goal pose is described as a complete hand pose. We evaluate the cost of a state \mathcal{S}_k based on the average spatial deviation between the target mesh $\mathbf{x}_{\text{target}}$ and the current solution \mathbf{x}_k . The spatial cost η_s is defined as

$$\eta_s = \|\mathbf{x}_k - \mathbf{x}_{\text{target}}\|_{L_{2,1}}^2. \quad (2)$$

On the physical robot, we have to connect tendons to the motors and sew tendons into the glove. This implies that one end of each tendon has to be pinned to the wrist and tendons should not be too erratic to minimize friction. To ensure these two conditions we additionally introduce the following constraints to our algorithm:

- The first node of each tendon has to run through a pinned node at the base of the mesh

- An additional regularizer cost term is introduced that penalizes large curvatures of tendons:

$$\eta_r = T_k^{\lambda_{r_0}}. \quad (3)$$

The total cost η_t of a state is therefore defined by

$$\eta_t = \lambda_s \eta_s + \lambda_r \eta_r \quad (4)$$

with λ_s , λ_{r_0} , and λ_r serving as hyper-parameters.

Acceptance of New States. New tendon routings and contractions are either accepted or rejected based on their total cost η_t . We implement a typical acceptance criterion for simulated annealing that always accepts a new state if their cost is lower than the cost of the previous state. The probability ϕ_{acc} of accepting an uphill move depends on the temperature T and the magnitude of the cost difference $\Delta_\eta = \eta_t(\mathbf{x}_{k+1}, \mathcal{T}_{k+1}) - \eta_t(\mathbf{x}_k, \mathcal{T}_k)$ resulting in

$$\phi_{\text{acc}}(\eta_{t,k}, \eta_{t,k+1}, T) = e^{-\frac{\Delta_\eta}{T}}. \quad (5)$$

Meta-Structure of Algorithm. To be able to generate designs quickly we run our optimization on multiple CPUs. Depending on the number of available CPUs we initialize a number of N particles that each run the same algorithm. Each particle is initialized independently with a random tendon routing and contraction. We allow particles to share their current best solution with other particles after a number of N_{epoch} iterations. We use the size of the neighborhood and the length of each epoch to balance the level of exploration and exploitation of the design space.

7. Tendon Routing User Study

To allow users (and ourselves) to experiment with tendon routings, we created a user interface on top of the finite element simulation. Our interface contains the following features. Users can (1) pick nodes and drag the mesh into desired configurations to create target poses; (2) quickly pick a set of nodes along which tendons are routed; (3) add, alter and remove tendons from the design; (4) create hand motions by contracting tendons; and (5) record and play back the created motion sequences.

To evaluate the difficulty of manually specifying tendon routing and to gather ground truth for the tendon optimization, we asked 20 participants without a soft robotics background to find tendon routings for a soft foam hand in simulation in order to enable that hand to achieve a certain target pose. We asked each of the 20 participants to create tendon routings and contractions for five grasps (Lateral Tripod Power Grasp, Medium Wrap Power Grasp, Prismatic 3-Finger Precision Grasp, Keypinch Power Grasp, Writing Tripod Precision Grasp). For each pose we set a time limit of 10 min and participants were allowed to place up to 10 tendons per grasp. Figure 5 depicts the general setup of the graphical user interface and shows the 5 target grasps.

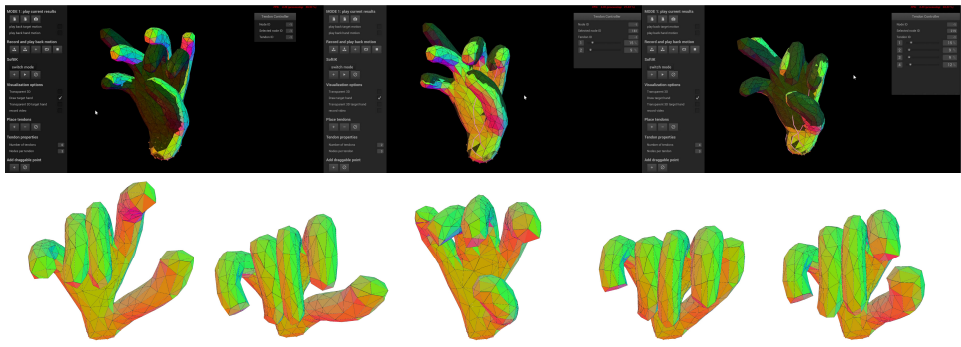


Fig. 5. (Top) Screencast of a user creating an exemplary tendon routing. The user's task is to place and contract tendons to match the target hand pose (depicted in darker colors). The current pose of the simulation mesh is shown in bright colors. Within the sequence, the user places four tendons on the mesh and selects contraction levels using the slider toolbar on the top right. (Bottom) Target grasps from left to right: Lateral Tripod Power Grasp, Medium Wrap Power Grasp, Prismatic 3-Finger Precision Grasp, Keypinch Power Grasp, Writing Tripod Precision Grasp.

8. Experiments and Results

Repeatability. To test repeatability of the foam manufacturing process, a planar two-fingered hand, shown in Fig. 6 (left) was fitted with a glove and 4 tendons: 2 flexors and 2 extensors per finger. Using a camera, the trajectories for 6 different grasps were recorded for 800 trials each. The first 50 trials were discarded as a “break-in” period. From the remaining 750 trials, 50 random trials for each of the 6 grasps were selected for analysis. Seven black dots 6 mm in diameter were attached along the gripper before testing to be used for motion tracking. The dots were tracked by applying a *Grayscale Conversion*, *Gaussian Blur*, *Prewitt Edge Filter*, and *Hough Circle Transform*, in sequence, to each frame. Then the circles were sorted using *Nearest Neighbors*. The final fingertip positions, p_{gt} , were recorded for each grasp, $g \in \{1, 2, \dots, 6\}$, and trial, $t \in \{1, 2, \dots, 50\}$. The nominal positions for each grasp were taken as the mean over the trials, $\bar{p}_g = (\sum_{i \in t} p_{gi})/50$. The error was

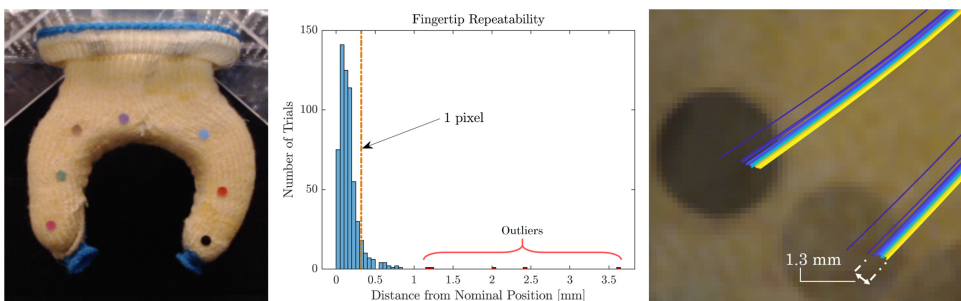


Fig. 6. (Left) Planar gripper with markers. (Middle) Histogram of fingertip repeatability over 600 trials. (Right) The fingertip position was observed to drift (shown as blue to yellow) over 8000 grasps.

Table 2. Repeatability statistics for planar gripper.

Values in [mm]	μ	σ	median	Max
All trials	0.1738	0.2293	0.1307	3.6360
Inlier trials	0.1576	0.1210	0.1296	0.8160

computed as the L^2 distance of the fingertips from their nominal positions, $e_{gt} = \|\bar{p}_g - p_{gt}\|_2$. The histogram of errors for all 600 trials is shown in Fig. 6 (middle). Upon inspection there appears to be several outliers in the data; we believe that these correspond to the rare instance that motor commands are not delivered due to a faulty serial connection, and that in the future this can be avoided with a simple program loop to verify motor command delivery. The distribution metrics for the complete data and inlier data (computed with the very conservative $\mu \pm 3\sigma$ filter) are given below in Table 2. In the future, higher resolution motion capture should be used, as many of the error measurements were sub-pixel in length. Finally, by plotting the fingertip locations in order, we notice some drift across the 800 trials, on the order of tenths of millimeters as shown in Fig. 6 (right). We believe that this is due to some yield, i.e., stretch, in the textile components, and can be reduced in the future by using stronger yarn in the glove knitting process.

Strength of the Foam Hands. To test strength of the foam hand, caging grasps were performed on a tennis ball with two separate hands. The pullout force was measured to be 3.2 N and 5.8 N, respectively, test setup is shown in Fig. 7. The difference in strength is primarily due to the hand geometries, in that grasp failure occurred due to foam compression rather than lack of tendon strength (i.e., motor torque) indicating that a more “opposable” thumb is important for power grasps.

Validation of the FEM Simulation Model. To quantify the accuracy of our simulation framework, we compare fingertip trajectories of a simulated and a physical foam hand robot. The deformations of the foam are tracked using a Vicon Motion Capture system. The physical foam hand robot used in this experiment is a nonanthropomorphic hand with four fingers and 10 tendons. Each finger is controlled by a pair of antagonistically routed tendons acting as flexor and extensor. In order to introduce abduction and adduction motions, we placed two additional tendons on



Fig. 7. The strength of caging grasps was measured by pulling on a grasped tennis ball until grasp failure.

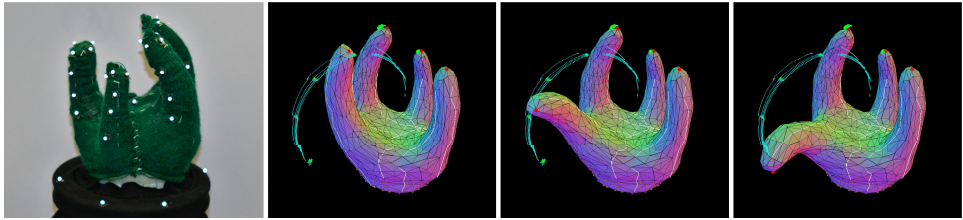


Fig. 8. (Left) Four-fingered hand with Vicon markers. (Left center-right) Simulated hand and motion capture trajectories for an extensor tendon moving from 10% (left center) to 50% (right) tendon contraction. Fingertip positions recorded by the Vicon system at each contraction level are averaged over all five trials and marked as green dots, fingertip positions of the simulation model are marked as red dots.

the left and right side of one finger. We record fingertip trajectories of our four-fingered foam hand using a Vicon motion capture system with 12 cameras. To get a robust estimate of the position and to prevent occlusions we place four markers around each fingertip as shown in Fig. 8, left. For registration purposes we additionally place markers on the platform on which the hand is mounted and alongside each finger. After the experiment the recorded markers are registered on the 3d mesh. This is done using a standard ICP algorithm. We define each fingertip position \mathbf{p}_j with $j = \{1, \dots, 4\}$ as the mean of the corresponding markers k with $k = \{1, \dots, 4\}$, with a distal offset of 5 mm normal to the plane spanned by the four markers: $\mathbf{p}_j = \frac{1}{4} \cdot \sum_{k=1}^4 \mathbf{p}_{jk} + 0.005 \cdot \mathbf{n}_j$. The RMS error describing the euclidean distance between the aligned point clouds of our ICP registration was 4.05 mm.

In terms of material parameters for the FEM simulation (mass density ρ , Young's modulus E , Poisson's ratio ν) we used the values found in Table 1.

We ran 5 trials in which each tendon is repeatedly contracted from 0% to 50% of its rest length in steps of 10%. The tendon rest length is distinct for each tendon and is computed in simulation.

A motion sequence of a contracting extensor tendon moving the simulated hand through the waypoints at 10%, 30%, and 50% contraction is shown in Fig. 8. The mean position error for all fingers including all activation levels is 0.626 cm. For each individual finger median error and the quartile deviations converge to similar values at all contraction levels. This suggests that even large deformations do not significantly decrease the accuracy of our model. In general we identify the following sources of position errors: (1) small deviations between tendon routings in simulation and reality; (2) tendon slack; (3) registration errors in motion capture system; (4) friction between tendon and glove; and (5) slight relative movements of foam core and glove during actuation. Most of these errors can be mitigated during fabrication of the hand, for example by using teflon-coated tendons or different gluing techniques. The results of this evaluation suggest that our model predicts foam deformations sufficiently well for simulation based learning of mapping from desired pose to tendon actuation.

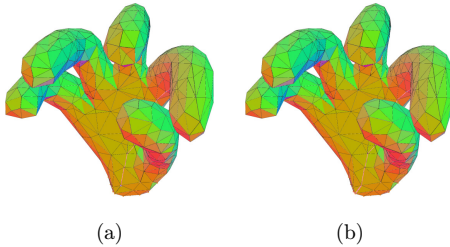


Fig. 9. Optimization result for a target pose created by contracting one tendon on the index finger. (a) Target pose and (b) Pose found by optimization.

Table 3. Tendon optimization hyper-parameters used for adjacency depth and regularizer cost term.

D	λ_{r0}	λ_s	λ_r
4	5.0	1.0	1.35

Tendon Optimization Results. First, we verify that the optimization successfully finds optimal solutions to our problem by manually placing and contracting one tendon on the index finger of the mesh and using the resulting pose as a target. Given the target mesh depicted in Fig. 9(a) the optimization yields exactly the same tendon and contraction that was used to create the target.

In order to achieve a wide variety of grasps we then optimize 10 tendons for 6 different poses (Ventral Power Grasp, Palmar Power Grasp, Lateral Tripod Power Grasp, Writing Tripod, Power Sphere Grasp, Prismatic 3-finger Precision Grasp) that have been recorded using the CyberGlove of the telemanipulation system described in Sec. 5. We use the hyper-parameters presented in Table 3. The solution we obtain consists of a tendon routing and 6 corresponding sets of contraction levels for each pose.

We build the physical robot based on our fabrication process introduced in Sec. 3 and transfer the contraction length l_c to motor activation levels M in degrees according to

$$M = \frac{(l_0 - l_c)}{\pi d_p} 360^\circ \quad (6)$$

with the tendon rest length l_0 and the pulley diameter d_p .

The physical robot can closely match the poses created by our optimization in simulation as shown in Fig. 10. With this hand we were able to successfully execute two of the 6 target grasps, the lateral tripod and the writing tripod (Fig. 11).

User Study Results. Figure 13 shows a compilation of poses created by users and the optimization. Column (I) hereby depicts the target pose while column (II) shows an overlay of all poses created by users for each target grasp. User-created poses with

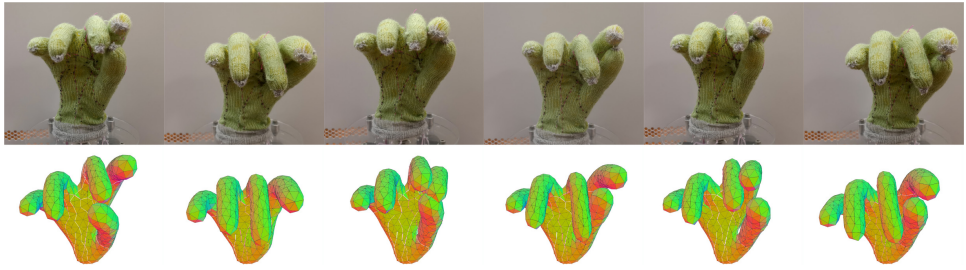


Fig. 10. Poses generated by tendon routing optimization in simulation (bottom) and on the physical foam hand robot (top).

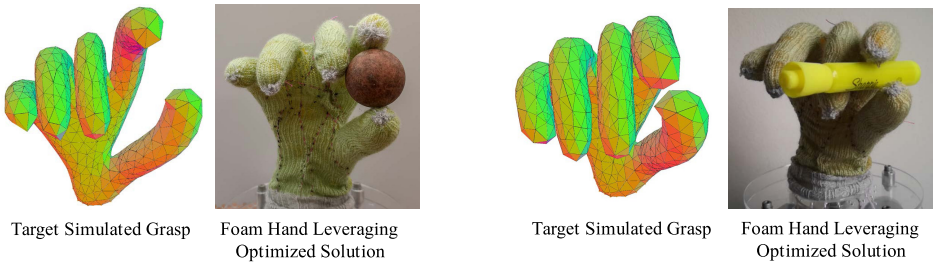


Fig. 11. Two examples of target grasps and the corresponding foam hands obtained by tendon optimization.

the lowest spatial deviation from the target pose and poses resulting from optimization are depicted in column (III) and (IV), respectively. Column (V) and (VI) show the rest pose of the mesh with the average deviation from the target encoded in color. Based on the color distribution shown in (V) and (VI) it can be observed that

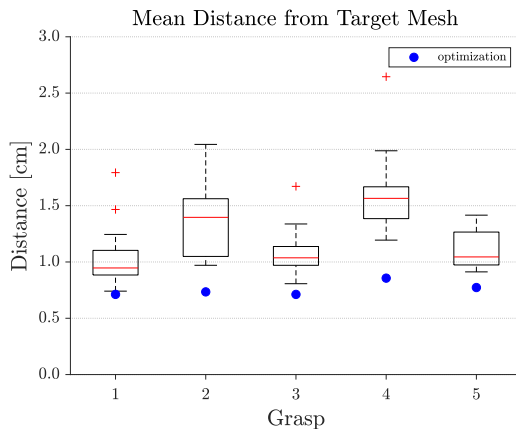


Fig. 12. Distribution of mean distance of nodes from target pose for all poses created by users in the study. The mean nodal distance achieved by the optimization is plotted as a blue dot. (1) Lateral Tripod, (2) Medium Wrap, (3) Prismatic, (4) Keypinch and (5) Writing Tripod.

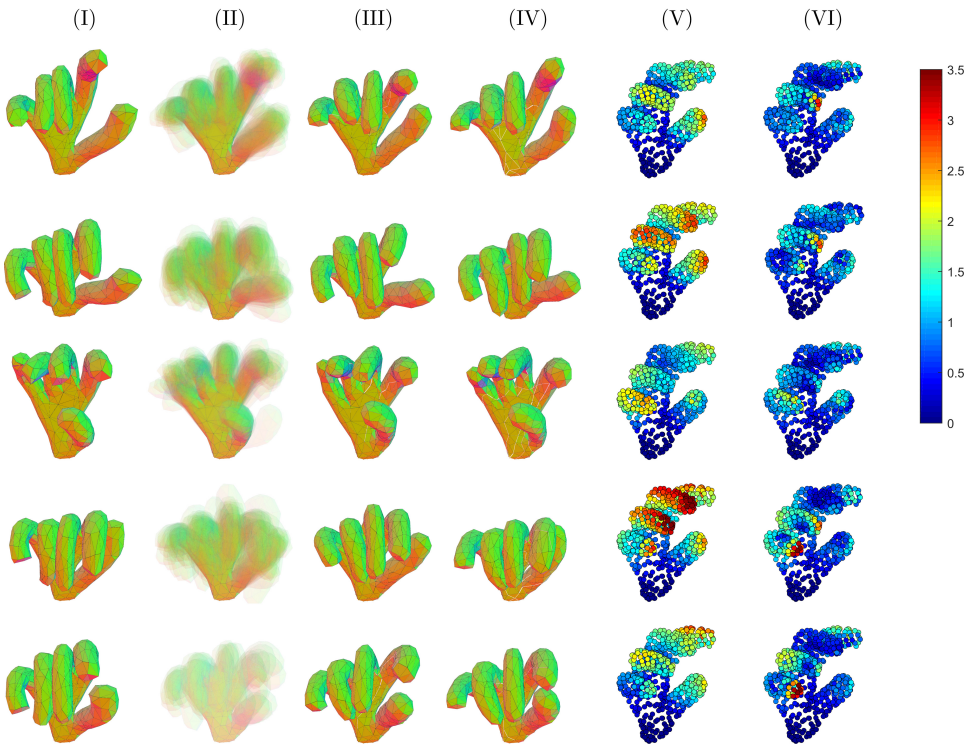


Fig. 13. (I) Target poses, (II) overlayed visualization of all poses created by the test subjects, (III) best user result, (IV) optimization result, (V) mean distance error of user-created poses in cm, and (VI) mean distance error of optimized poses in cm.

solutions found through optimization are matching the target poses more closely and do not tend to give precedence to specific nodes. Interestingly, participants of the user study, seem to infer which fingers are important for a successful grasp based on the pose, although they had no knowledge of the intended grasp. This can be best observed based on the Keypinch grasp [Fig. 13, (V), row 4] for which the average error of middle finger, ring finger and pinky is remarkably higher than for the thumb and index finger. Overall we observed a large variance in terms of quality of user designs. Figure 12 shows that some participants seem to have a good intuition on how the mesh deforms when tendons are contracted while others found it more difficult to design suitable tendon routings. For all targets the optimization outperformed even the best tendon routings created in the user study. The quantitative errors can be found in Table 4.

Manipulation Showcase. Figure 1, bottom shows a collection of hands which we have manufactured using this process. Figure 14 shows several static grasps, and Fig. 15 shows several in-hand manipulations.

Table 4. Comparison of user study results (S) and optimization (O) based on the mean distance error of nodes from target pose for each grasp type.

Grasp type	S [cm]	O [cm]
Lateral tripod	1.03	0.71
Medium wrap	1.36	0.73
Prismatic 3-finger	1.08	0.71
Keypinch	1.60	0.86
Writing tripod	1.11	0.77

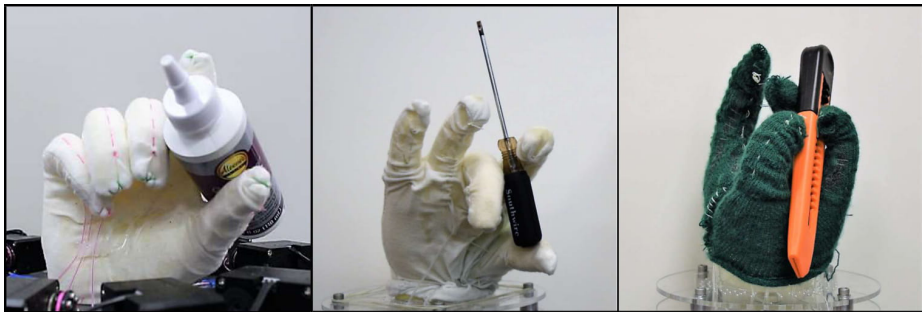


Fig. 14. Demonstration of static grasping with a glue bottle (left), a screwdriver (middle) and a box cutter (right).

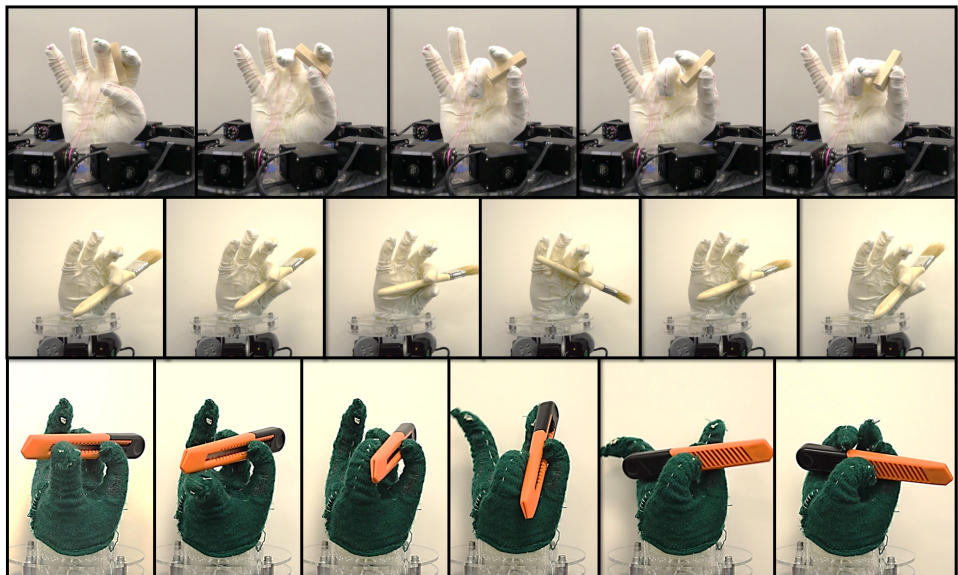


Fig. 15. In-hand manipulation sequences of three foam robots. (Top) Lateral Grasp Transition. (Middle) Rocking Motion. (Bottom) Utility Knife Spinning.

9. Discussion

This paper has described an end-to-end process of design, optimization, manufacturing and control of soft foam robot hands. Several of the showcased manipulations were performed with the first prototype ever made, before improving designs; still the robot is capable of achieving robust motions and in-hand manipulations right-away without the need to worry about self-collisions, a capability not yet seen in truly soft robotic hands.

Several of the grippers presented have been in use for over one year and thousands of trials, additionally they have been transported transcontinentally in checked luggage and exposed to harsh weather conditions, all without a noticeable lack in performance. While this information is anecdotal, it is the opinion of the authors that these grippers demonstrate good longevity and ruggedness overall.

Learning. Linear regression was sensible for learning on the real robot due to the extremely small amount of data available. It is a simple and straightforward model, and performed well in practice, both for poses that were not part of the training set and when teleoperating real-world grasping and manipulation tasks.

When we moved to the simulation environment, we found that more complex models — and even nearest neighbor — appeared to outperform linear regression. We experimented extensively in simulation with direct control using supervised learning, and we found that it behaved smoothly and intuitively in most cases. We believe, however, that linear regression can still work well in the simulation environment, but that test poses should be selected carefully to cover typical use cases (as was done in the real-robot learning).

Effects of Different Tendon Routings. Since soft robots do not have any joints, the variety and complexity of achievable poses largely depends on the tendon routing. We explore the effects of different routings in simulation by utilizing FEM tuned to match the behavior of the foam and apply them on the physical hand. A major weakness of our initial design is the inability of the thumb to abduct and oppose the palm. This is mainly caused by an inefficient tendon routing with two antagonistic tendons. Changing the routing increased the complexity of feasible motions of the thumb significantly.

Depending on the task, multi-fingered hands are required to achieve certain grasps and motions. The motions of the hand are most importantly determined by the tendon routing. This feature highlights an important advantage of our tendon driven approach, compared to, e.g., pneumatically actuated designs, because of the ability to change the kinematics any time by switching to another tendon routing by re-sewing the tendons or swapping gloves, $a \sim 1\text{ h}$ process.

Robot Rest Pose. Our experiments show that the rest pose of the hand design pre-defines the range of motion independently of the tendon arrangement. Since the shape of the foam is fixed and cannot be changed (unlike the tendons), evaluating the geometry in simulation is an important step before fabricating the actual foam

model. Depending on the underlying task, certain poses are identified to be more suitable than others. This especially applies to human-like hand geometries. We discovered that human-like hands with flat rest poses have a problem grasping large objects such as tennis balls. This is due to the inability of the fingers to curl around the object and oppose the palm. An advantage of flat rest poses over curled rest poses is that they do not need tendons that run on the back of the hand, because the geometry and the compliance of the foam itself restores the hand to its original shape. This makes it possible to add more tendons to the front of the fingers increasing the overall dexterity of the design.

Additionally, aspects of the robot geometry are important to consider. It was observed that relatively thick palms and fingers lead to (possibly undesired) localized stiffening. These undesired features can be mitigated by iteratively changing the hand designs and testing them in simulation, reducing the need for iteration of the physical prototypes.

Simulation brings advantages of being able to iterate and test in a rapid manner. Based on our validation experiments, we are confident in being able to test tendon routings and iterate on different hand geometries and tendon designs in rapid fashion. However, designing tendon routings remains a challenging and nonintuitive task, especially if a hand must reach a specific range of poses to accomplish some goal task. To overcome this challenge we apply a tendon optimization algorithm which automatically determined the ideal setup using our simulation framework.

Assisted design of compliant hand morphologies. While designing new soft hand models from scratch, we found that certain types of grasps could often times not be achieved due to short or misplaced fingers or inefficient rest poses. For example, if one desires to build a soft hand that is able to pick up apples, the fingers of the hand should be long enough to properly enclose the apple to firmly grasp it. In the case of an anthropomorphic hand morphology, the foam should thus be able to assume a shape which enables similar contact points and configurations as they occur when humans grasp an apple. This means to design a foam hand morphology that is able to assume a kinematically equivalent pose when grasping an apple one needs to consider the positions of the thumb, fingers, palm and their proportions. We found that without a proper reference that constrains the continuous design space of the foam it is impractical to produce purposeful designs. Therefore, we establish a process that supports the design of task specific hand rest shapes, which “grows” a new hand mesh along a set of 3D feature points.

We obtain these feature points using a CyberGlove and the virtual human hand model provided by the CyberGlove SDK. For a given pose, 3D positions of the MCP, PIP, and DIP joints and the distal end of the distal phalanges are recorded. An exemplary depiction of the resulting points is given in Fig. 16(a).

In a second step we subsequently connect the base of the palm to the recorded joint positions, representing their coordinates in a 3D grid. We then further increase the volume of this structure by iteratively dilating occupied points towards

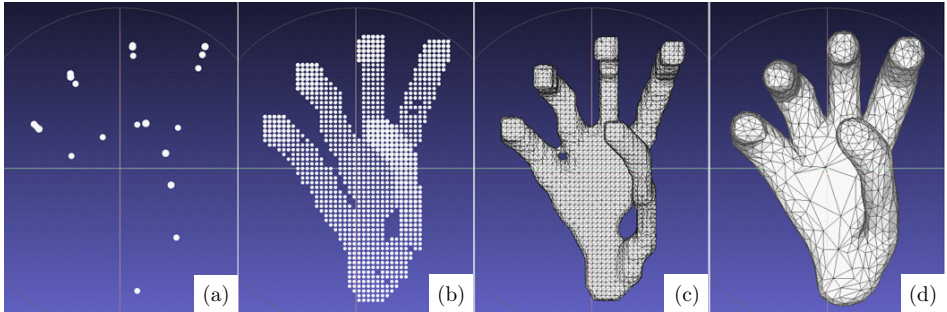


Fig. 16. “Growing” a new hand mesh along recorded joint positions. (a) 3D joint positions recorded using a CyberGlove. (b) Pointcloud obtained by path planning between the points. (c) A rough surface mesh created by surface reconstruction. (d) The resulting smoothed hand mesh.

directions of unoccupied grid points [Fig. 16(b)]. In this example, a grid resolution of $200 \times 200 \times 200$ with a cell size of $3 \times 3 \times 3$ mm is used and a total of two dilation operations were executed. Then the Delaunay tetrahedralization of the set of 3D points is calculated using *tetgen*.⁷¹ The resulting convex hull is then shaped using an alpha shaping algorithm [Fig. 16(c)]. As a final step we apply Laplacian smoothing⁷² and adjust the mesh resolution using *MeshLab*.⁷³ It is possible to refine or coarsen the mesh depending on the required accuracy of the simulation. This naturally is a trade-off between simulation speed and accuracy. Meshes that we created for the purpose of optimization typically consisted of 1000–2000 nodes.

Weaknesses and Current Limitations. A limitation of the current design is the low stiffness of the foam, which limits the forces we can apply during manipulation, especially while performing “pushing” or “pressing” actions. Our goal is to address this issue in future work by embedding controllable stiffness elements. Additionally, the foam has some hysteresis when returning to the rest pose which we postulate to be caused by tendon-glove friction, this can likely be mitigated with a corrective maneuver, i.e., extending beyond the rest pose in the opposite direction.

The current method of routing tendons along the glove limits the possibilities of these hands two-fold. (1) Geometrically: routing tendons through the foam body would allow for more motions and increased forces by the hands. Initial attempts to route tendons through the foam caused tearing, we would like to explore improved methods to accomplish this in future work. (2) Mechanically: the tendons pull on the gloves, straining the adhesive layer, limiting the maximum tendon forces that can be applied without failure. First attempts at using gloves had no adhesive, causing the gloves to slip. We also experimented with cyanoacrylate, which caused foam hardening. As for the foam itself, it was chosen for being easy to work with. Nevertheless, there are many high performance textiles, adhesives, and specifically engineered foams which could be used instead, and these will likely further improve the longevity, durability, and performance of these soft multi-fingered hands.

Our current control approach does not feature any sensors, which would be required for closed-loop control and to improve the overall control accuracy. While adding sensors to our foam hands lies beyond the scope of this paper we reserve this for future work.

In terms of optimizing foam hands, our current approach only optimizes for tendon routings and contraction levels while the morphology and the rest shape of the hands are not considered. After transferring the tendon routings found in simulation to the physical robot we were able to successfully execute 2/6 grasps. While this demonstrates that there is a gap between simulation and reality, we believe that a large portion of the gap is caused by the optimization goals themselves, which only consist of discrete static poses that do not include contact points with objects or forces. Incorporating dynamic object interactions into our simulation framework will therefore likely further improve the grasping capabilities of optimized soft foam hands.

10. Conclusions

We have introduced fully soft foam robots and their applications to robotic manipulation. In this work, we have covered our fabrication, control, and optimization methodologies and have showcased a number of experiments and demonstrations that speak to their capabilities in the robotic manipulation space. We believe that this work serves as a promising introduction to this technology, that we are excited to see grow and evolve in the coming years.

Acknowledgments

This work was supported in part by the National Robotics Initiative Grant NSF IIS-1637853 and in part by a NASA Space Technology Research Fellowship (Award 80NSSC17K0140). Any opinions, figures, and conclusions or recommendations expressed in this material are those of the authors and do not necessarily reflect the views of the National Robotics Initiative or NASA. This work used the Extreme Science and Engineering Discovery Environment (XSEDE).

We thank James McCann and Vidya Narayanan for knitting our gloves. Furthermore we want to thank Ella Moore for assisting us with fabricating soft foam hands.

Dominik Bauer, Cornelia Bauer and Jonathan P. King contributed to this work equally.

References

1. J. P. King, D. Bauer, C. Schlagenhauf, K.-H. Chang, D. Moro, N. Pollard and S. Coros, Design, fabrication, and evaluation of tendon-driven multi-fingered foam hands, *2018 IEEE RAS Int. Conf. Humanoid Robots* (IEEE, Beijing, China, 2018), pp. 1–9.
2. C. Schlagenhauf, D. Bauer, J. P. King, K.-H. Chang, D. Moro, S. Coros and N. Pollard, Control of tendon-driven soft foam robot hands, *2018 IEEE RAS Int. Conf. Humanoid Robots* (Beijing, China, 2018), pp. 1–7.

3. S. Hirose and Y. Umetani, The development of soft gripper for the versatile robot hand, *Mech. Machine Theo.* **13**(3) (1978) 351–359.
4. S. Sanan, J. B. Moidel and C. G. Atkeson, Robots with inflatable links, *2009 IEEE/RSJ Int. Conf. Intelligent Robots and Systems* (St. Louis, MO, USA, 2009), pp. 4331–4336.
5. C. D. Kidd, W. Taggart and S. Turkle, A sociable robot to encourage social interaction among the elderly, *2006 IEEE Int. Conf. Robotics and Automation*, 2006, IEEE, pp. 3972–3976.
6. D. Rus and M. T. Tolley, Design, fabrication and control of soft robots, *Nature* **521**(7553) (2015) 467.
7. W. D. Stiehl, C. Breazeal, K.-H. Han, J. Lieberman, L. Lalla, A. Maymin, J. Salinas, D. Fuentes, R. Toscano, C. H. Tong *et al.*, The huggable: A therapeutic robotic companion for relational, affective touch, *ACM SIGGRAPH 2006 Emerging Technologies* (ACM, 2006), p. 15.
8. R. Deimel and O. Brock, A novel type of compliant and underactuated robotic hand for dexterous grasping, *The Int. J. Robot. Res.* **35**(1–3) (2016) 161–185.
9. R. F. Shepherd, F. Ilievski, W. Choi, S. A. Morin, A. A. Stokes, A. D. Mazzeo, X. Chen, M. Wang and G. M. Whitesides, Multigait soft robot, *Proc. National Academy of Sci.* **108**(51) (2011) 20400–20403.
10. Soft robotics inc., <https://www.softroboticsinc.com/team/>, Accessed on 10 September, 2017.
11. S. Seok, C. D. Onal, K.-J. Cho, R. J. Wood, D. Rus and S. Kim, Meshworm: A peristaltic soft robot with antagonistic nickel titanium coil actuators, *IEEE/ASME Trans. Mechatron.* **18**(5) (2013) 1485–1497.
12. M. T. Tolley, R. F. Shepherd, B. Mosadegh, K. C. Galloway, M. Wehner, M. Karpelson, R. J. Wood and G. M. Whitesides, A resilient, untethered soft robot, *Soft Robot.* **1**(3) (2014) 213–223.
13. C. M. Donatelli, Z. T. Serlin, P. Echols-Jones, A. E. Scibelli, A. Cohen, J.-M. Musca, S. Rozen-Levy, D. Buckingham, R. White and B. A. Trimmer, Soft foam robot with caterpillar-inspired gait regimes for terrestrial locomotion, *2017 Int. Conf. Intelligent Robots and Systems (IROS)*, 2017, IEEE, pp. 476–481.
14. P. Polygerinos, Z. Wang, K. C. Galloway, R. J. Wood and C. J. Walsh, Soft robotic glove for combined assistance and at-home rehabilitation, *Robot. Autonomous Syst.* **73** (2015) 135–143.
15. C. J. Payne, I. Wamala, C. Abah, T. Thalhofer, M. Saeed, D. Bautista-Salinas, M. A. Horvath, N. V. Vasilyev, E. T. Roche, F. A. Pigula and C. J. Walsh, An implantable extracardiac soft robotic device for the failing heart: Mechanical coupling and synchronization, *Soft Robot.* **4**(3) (2017) 241–250.
16. P. Polygerinos, S. Lyne, Z. Wang, L. F. Nicolini, B. Mosadegh, G. M. Whitesides and C. J. Walsh, Towards a soft pneumatic glove for hand rehabilitation, *2013 IEEE/RSJ Int. Conf. Intelligent Robots and Systems (IROS)* (Tokyo, Japan, 2013), pp. 1512–1517.
17. S. Mghames, M. Laghi, C. D. Santina, M. Garabini, M. Catalano, G. Grioli and A. Bicchi, Design, control and validation of the variable stiffness exoskeleton flexo, *2017 Int. Conf. Rehabilitation Robotics (ICORR)* (London, UK, 2017), pp. 539–546.
18. J. M. Bern, K.-H. Chang and S. Coros, Interactive design of animated plushies, *ACM Trans. Graphics (TOG)* **36**(4) (2017) 80.
19. J. M. Bern, G. Kumagai and S. Coros, Fabrication, modeling, and control of plush robots, *Int. Conf. Intelligent Robots and Systems* (Vancouver, Canada, 2017), pp. 3739–3746.
20. M. Cianchetti, M. Calisti, L. Margheri, M. Kuba and C. Laschi, Bioinspired locomotion and grasping in water: The soft eight-arm octopus robot, *Bioinspirat. Biomimetics* **10**(3) (2015) 035003.

21. R. Deimel and O. Brock, A compliant hand based on a novel pneumatic actuator, *2013 IEEE Int. Conf. Robotics and Automation* (Karlsruhe, Germany, 2013), pp. 2047–2053.
22. A. D. Marchese, C. D. Onal and D. Rus, Autonomous soft robotic fish capable of escape maneuvers using fluidic elastomer actuators, *Soft Robot.* **1**(1) (2014) 75–87.
23. M. Amjadi, K.-U. Kyung, I. Park and M. Sitti, Stretchable, skin-mountable, and wearable strain sensors and their potential applications: A review, *Adv. Funct. Mater.* **26**(11) (2016) 1678–1698.
24. M. Kaltenbrunner, T. Sekitani, J. Reeder, T. Yokota, K. Kuribara, T. Tokuhara, M. Drack, R. Schwödauer, I. Graz, S. Bauer-Gogonea *et al.*, An ultra-lightweight design for imperceptible plastic electronics, *Nature* **499**(7459) (2013) 458.
25. C. Larson, B. Peele, S. Li, S. Robinson, M. Totaro, L. Beccai, B. Mazzolai and R. Shepherd, Highly stretchable electroluminescent skin for optical signaling and tactile sensing, *Science* **351**(6277) (2016), 1071–1074.
26. Y. Park, B. Chen and R. J. Wood, Design and fabrication of soft artificial skin using embedded microchannels and liquid conductors, *IEEE Sensors J.* **12**(8) (2012) 2711–2718.
27. B. Gorissen, D. Reynaerts, S. Konishi, K. Yoshida, J.-W. Kim and M. De Volder, Elastic inflatable actuators for soft robotic applications, *Adv. Mater.* **29**(43) (2017) 1604977.
28. J. P. King, L. E. Valle, N. Pol and Y.-L. Park, Design, modeling, and control of pneumatic artificial muscles with integrated soft sensing, *2017 IEEE Int. Conf. Robotics and Automation (ICRA)*, 2017, IEEE, pp. 4985–4990.
29. B. Mosadegh, P. Polygerinos, C. Keplinger, S. Wennstedt, R. F. Shepherd, U. Gupta, J. Shim, K. Bertoldi, C. J. Walsh and G. M. Whitesides, Pneumatic networks for soft robotics that actuate rapidly, *Adv. Funct. Mater.* **24**(15) (2014) 2163–2170.
30. P. Ohta, L. Valle, J. King, K. Low, J. Yi, C. G. Atkeson and Y.-L. Park, Design of a lightweight soft robotic arm using pneumatic artificial muscles and inflatable sleeves, *Soft Robot.* **5**(2) (2018) 204–215.
31. R. Pelrine, R. Kornbluh, Q. Pei and J. Joseph, High-speed electrically actuated elastomers with strain greater than 100%, *Science* **287**(5454) (2000) 836–839.
32. M. Shahinpoor and K. J. Kim, Ionic polymer-metal composites: I. fundamentals, *Smart Mater. Struct.* **10**(4) (2001) 819.
33. J. Wirekoh and Y.-L. Park, Design of flat pneumatic artificial muscles, *Smart Mater. Struct.* **26**(3) (2017) 035009.
34. H. K. Yap, H. Y. Ng and C.-H. Yeow, High-force soft printable pneumatics for soft robotic applications, *Soft Robot.* **3**(3) (2016) 144–158.
35. E. Brown, N. Rodenberg, J. Amend, A. Mozeika, E. Steltz, M. R. Zakin, H. Lipson and H. M. Jaeger, Universal robotic gripper based on the jamming of granular material, *Proc. National Academy Sci.* **107**(44) (2010) 18809–18814.
36. M. R. Cutkosky, Climbing with adhesion: From bioinspiration to biounderstanding, *Interface Focus* **5**(4) (2015) 20150015.
37. J. Shintake, S. Rosset, B. Schubert, D. Floreano and H. Shea, Versatile soft grippers with intrinsic electroadhesion based on multifunctional polymer actuators, *Adv. Mater.* **28**(2) (2015) 231–238.
38. R. K. Katzschmann, A. D. Marchese and D. Rus, Autonomous object manipulation using a soft planar grasping manipulator, *Soft Robot.* **2**(4) (2015) 155–164.
39. A. D. Marchese, K. Komorowski, C. D. Onal and D. Rus, Design and control of a soft and continuously deformable 2d robotic manipulation system, *2014 IEEE Int. Conf. Robotics and Automation (ICRA)*, (Hong Kong, China, 2014), pp. 2189–2196.

40. R. V. Martinez, J. L. Branch, C. R. Fish, L. Jin, R. F. Shepherd, R. M. D. Nunes, Z. Suo and G. M. Whitesides, Robotic tentacles with three-dimensional mobility based on flexible elastomers, *Adv. Mater.* **25**(2) (2012) 205–212.
41. J. Zhou, S. Chen and Z. Wang, A soft-robotic gripper with enhanced object adaptation and grasping reliability, *IEEE Robot. Automat. Lett.* **2**(4) (2017) 2287–2293.
42. Z. Xu and E. Todorov, Design of a highly biomimetic anthropomorphic robotic hand towards artificial limb regeneration, *2016 IEEE Int. Conf. Robotics and Automation (ICRA)*, 2016, pp. 3485–3492.
43. J. Gafford, Y. Ding, A. Harris, T. McKenna, P. Polygerinos, D. Holland, A. Moser and C. Walsh, Shape deposition manufacturing of a soft,atraumatic, deployable surgical grasper, *J. Med. Devices* **8**(3) (2014), 030927.
44. R. Ma and A. Dollar, Yale openhand project: Optimizing open-source hand designs for ease of fabrication and adoption, *IEEE Robot. Automat. Magazine* **24**(1) (2017) 32–40.
45. L. U. Odhner, L. P. Jentoft, M. R. Claffee, N. Corson, Y. Tenzer, R. R. Ma, M. Buehler, R. Kohout, R. D. Howe and A. M. Dollar, A compliant, underactuated hand for robust manipulation, *The Int. J. Robot. Res.* **33**(5) (2014) 736–752.
46. M. Calisti, M. Giorelli, G. Levy, B. Mazzolai, B. Hochner, C. Laschi and P. Dario, An octopus-bioinspired solution to movement and manipulation for soft robots, *Bioinspirat. Biomimetics* **6**(3) (2011) 036002.
47. R. Mutlu, G. Alici, M. in het Panhuis and G. M. Spinks, 3d printed flexure hinges for soft monolithic prosthetic fingers, *Soft Robot.* **3**(3) (2016) 120–133.
48. H. Jiang, Z. Wang, X. Liu, X. Chen, Y. Jin, X. You and X. Chen, A two-level approach for solving the inverse kinematics of an extensible soft arm considering viscoelastic behavior, *2017 IEEE Int. Conf. Robotics and Automation (ICRA)*, (Singapore, 2017), pp. 6127–6133.
49. M. Rolf and J. J. Steil, Efficient exploratory learning of inverse kinematics on a bionic elephant trunk, *IEEE Trans. Neural Networks Learn. Syst.* **25**(6) (2014) 1147–1160.
50. T. G. Thuruthel, E. Falotico, M. Cianchetti and C. Laschi, Learning global inverse kinematics solutions for a continuum robot, *ROMANSY 21 — Robot Design, Dynamics and Control* (Cham), 2016, pp. 47–54.
51. F. J. Chen, S. Dirven, W. L. Xu and X. N. Li, Soft actuator mimicking human esophageal peristalsis for a swallowing robot, *IEEE/ASME Trans. Mechatronics* **19**(4) (2014) 1300–1308.
52. C. Duriez, Control of elastic soft robots based on real-time finite element method, *2013 IEEE Int. Conf. Robotics and Automation (ICRA)*, 2013, IEEE, pp. 3982–3987.
53. A. D. Marchese and D. Rus, Design, kinematics, and control of a soft spatial fluidic elastomer manipulator, *The Int. J. Robot. Res.* **35**(7) (2016) 840–869.
54. F. Saunders, B. A. Trimmer and J. Rife, Modeling locomotion of a soft-bodied arthropod using inverse dynamics, *Bioinspirat. Biomimetics* **6**(1) (2011) 016001.
55. M. Giorelli, F. Renda, M. Calisti, A. Arienti, G. Ferri and C. Laschi, Neural network and jacobian method for solving the inverse statics of a cable-driven soft arm with nonconstant curvature, *IEEE Trans. Robot.* **31**(4) (2015) 823–834.
56. R. Deimel, P. Irmisch, V. Wall and O. Brock, Automated co-design of soft hand morphology and control strategy for grasping, *2017 IEEE/RSJ Int. Conf. Intelligent Robots and Systems (IROS)*, (Vancouver, Canada, 2017), pp. 1213–1218.
57. J. Rieffel, D. Knox, S. Smith and B. Trimmer, Growing and evolving soft robots, *Artific. Life* **20**(1) (2014) 143–162.
58. J. Hiller and H. Lipson, Automatic design and manufacture of soft robots, *IEEE Trans. Robot.* **28**(2) (2012) 457–466.

59. J. M. Inouye and F. J. Valero-Cuevas, Anthropomorphic tendon-driven robotic hands can exceed human grasping capabilities following optimization, *The Int. J. Robot. Res.* **33**(5) (2014) 694–705.
60. A. C. Lin and N. H. Quang, Automatic generation of mold-piece regions and parting curves for complex cad models in multi-piece mold design, *Comput.-Aided Design* **57** (2014) 15–28.
61. Z. Zhou, S. Gao, Z. Gu and J. Shi, A feature-based approach to automatic injection mold generation, *Proc. Geometric Modeling and Processing 2000. Theory and Applications* (Hong Kong, China, 2000), pp. 57–68.
62. J. McCann, L. Albaugh, V. Narayanan, A. Grow, W. Matusik, J. Mankoff and J. Hodgins, A compiler for 3d machine knitting, *ACM Trans. Graphics (TOG)* **35**(4) (2016) 49.
63. Y. Seol, C. O’Sullivan and J. Lee, Creature features: Online motion puppetry for non-human characters, *Proc. 12th ACM SIGGRAPH/Eurographics Symp. Computer Animation SCA ’13* (ACM, New York, NY, USA, 2013), pp. 213–221.
64. M. Plappert, M. Andrychowicz, A. Ray, B. McGrew, B. Baker, G. Powell, J. Schneider, J. Tobin, M. Chociej, P. Welinder *et al.*, Multi-goal reinforcement learning: Challenging robotics environments and request for research, arXiv:1802.09464.
65. T. P. Lillicrap, J. J. Hunt, A. Pritzel, N. Heess, T. Erez, Y. Tassa, D. Silver and D. Wierstra, Continuous control with deep reinforcement learning, arXiv:1509.02971.
66. M. Andrychowicz, F. Wolski, A. Ray, J. Schneider, R. Fong, P. Welinder, B. McGrew, J. Tobin, O. P. Abbeel and W. Zaremba, Hindsight experience replay, *Advances in Neural Information Processing Systems* (Long Beach, CA, USA, 2017), pp. 5048–5058.
67. Autodesk remake, <https://www.autodesk.com/products/remeake/overview>, Accessed on 19 July, 2017.
68. Tetgen, <http://wias-berlin.de/software/tetgen/>, Accessed on 19 July, 2017.
69. N. Metropolis, A. W. Rosenbluth, M. N. Rosenbluth, A. H. Teller and E. Teller, Equation of state calculations by fast computing machines, *The J. Chem. Phys.* **21**(6) (1953) 1087–1092.
70. N. Metropolis and S. Ulam, The monte carlo method, *J. Am. Statistic. Assoc.* **44**(247) (1949) 335–341.
71. H. Si, Tetgen, a delaunay-based quality tetrahedral mesh generator, *ACM Trans. Math. Softw.* **41**(2) (2015) 11:1–11:36.
72. O. Sorkine, D. Cohen-Or, Y. Lipman, M. Alexa, C. Rössl and H.-P. Seidel, Laplacian surface editing, *Proc. 2004 Eurographics/ACM SIGGRAPH Symp. Geometry Processing* (Nice, France, 2004), pp. 175–184.
73. P. Cignoni, M. Callieri, M. Corsini, M. Dellepiane, F. Ganovelli and G. Ranzuglia, MeshLab: An open-source mesh processing tool, *Eurographics Italian Chapter Conf.* (Salerno, Italy, 2008), pp. 129–136.



Dominik Bauer received his M.S. degree in Mechanical Engineering from Karlsruhe Institute of Technology in 2018. For his Master’s thesis he performed research on the design optimization of soft robotic hands in the Robotics Institute at Carnegie Mellon University. In 2019, Dominik will continue his research in the field of soft robotics at CMU as a Ph.D. candidate.



Cornelia Bauer graduated with a M.S. degree in Mechanical Engineering from Karlsruhe Institute of Technology in 2018. She currently works on policy optimization for industrial manipulation at the Bosch Research Technology Center in Sunnyvale. Before that, Cornelia performed research on the modeling and control of soft robotic hands at Carnegie Mellon University. She will join the Robotics Institute as PhD candidate in 2019 to continue her research.



Jonathan P. King is currently a NASA Fellowship (NSTRF 2017) supported Ph.D. Candidate at the Robotics Institute at Carnegie Mellon University. His research focuses broadly on robotic manipulation. Before coming to CMU, Jonathan was a Robotics Mechanical Engineer at the NASA Jet Propulsion Laboratory from 2013–2015. Before that he graduated with a B.S. degree in Mechanical Engineering from The Ohio State University in 2013 where he received the Outstanding Undergraduate Research Award.



Daniele Moro will graduate with a B.S. degree in Computer Science from Boise State University in 2020. He is currently an Undergraduate Student Researcher, working on visual reference resolution and multimodal embodied semantics. Daniele is a Barry Goldwater Scholar, a Carnegie Mellon Robotics Institute Summer Scholar, a Kleiner Perkins Engineering Fellow, and a CRA Outstanding Undergraduate Researcher Finalist.



Kai-Hung Chang received his M.S. degree in Robotics from Carnegie Mellon University in 2018 and a Bachelor degree in Physics from National Taiwan University. He is currently a Research Scientist at Autodesk Research. At CMU, he started his research studying computational design of soft robots aided by physics-based simulation. His research interests include the development and application of general machine learning, robotics, and VR/AR.



Stelian Coros is an Assistant Professor in the Department of Computer Science at ETH Zurich, where he leads the Computational Robotics Lab (CRL). He is also an Adjunct Professor in the Robotics Institute at Carnegie Mellon University. Stelian received his Ph.D. in Computer Science from the University of British Columbia in 2011. His work bridges the fields of Visual Computing, Robotics and Computational Fabrication.



Nancy Pollard is a Professor in the Robotics Institute and the Computer Science Department at Carnegie Mellon University. She received her Ph.D. in Electrical Engineering and Computer Science from the MIT Artificial Intelligence Laboratory in 1994, where she performed research on grasp planning for articulated robot hands. Before joining CMU, Nancy was an Assistant Professor and part of the Computer Graphics Group at Brown University. She received the NSF CAREER award in 2001 for research on “Quantifying Humanlike Enveloping Grasps” and the Okawa Research Grant in 2006 for “Studies of Dexterity for Computer Graphics and Robotics”.